

# Single-molecule Force Spectroscopy Predicts a Misfolded, Domain-swapped Conformation in human $\gamma$ D-Crystallin Protein\*

Received for publication, June 26, 2015, and in revised form, December 22, 2015. Published, JBC Papers in Press, December 24, 2015, DOI 10.1074/jbc.M115.673871

 Sergi Garcia-Manyes<sup>†1</sup>, David Giganti<sup>§</sup>, Carmen L. Badilla<sup>§</sup>, Ainhoa Lezamiz<sup>‡</sup>, Judit Perales-Calvo<sup>‡</sup>, Amy E. M. Beedle<sup>‡</sup>, and Julio M. Fernández<sup>§</sup>

 From the <sup>†</sup>Department of Physics and Randall Division of Cell and Molecular Biophysics, King's College London, London WC2R 2LS, United Kingdom and the <sup>§</sup>Department of Biological Sciences, Columbia University, New York, New York 10027

Cataract is a protein misfolding disease where the size of the aggregate is directly related to the severity of the disorder. However, the molecular mechanisms that trigger the onset of aggregation remain unknown. Here we use a combination of protein engineering techniques and single-molecule force spectroscopy using atomic force microscopy to study the individual unfolding pathways of the human  $\gamma$ D-crystallin, a multidomain protein that must remain correctly folded during the entire lifetime to guarantee lens transparency. When stretching individual polypeptides containing two neighboring H $\gamma$ D-crystallin monomers, we captured an anomalous misfolded conformation in which the  $\beta$ 1 and  $\beta$ 2 strands of the N terminus domain of two adjacent monomers swap. This experimentally elusive domain-swapped conformation is likely to be responsible for the increase in molecular aggregation that we measure *in vitro*. Our results demonstrate the power of force spectroscopy at capturing rare misfolded conformations with potential implications for the understanding of the molecular onset of protein aggregation.

Protein misfolding and aggregation have been identified as critical biochemical processes underlying the pathology of a variety of increasingly prevalent human diseases, including amyotrophic lateral sclerosis (1) and antitrypsin deficiency (2). For a number of these conditions, domain swapping has been proposed as the mechanism of the off-pathway aggregation reaction (3, 4). Lens cataract is one of the most conspicuous protein misfolding diseases, affecting nearly 50% of the population over 75 years of age, and is the leading cause of blindness in the world (5). Crystallins, which are synthesized *in utero*, comprise 90% of proteins in the mature lens and guarantee its trans-

parency (6–9). These singular physiological conditions impose severe stability constraints on the crystallin proteins, whose functionality relies on the retention of a life-long soluble, folded state (10).

Cataractous lenses extracted surgically from the human eye contain insoluble species that include the three main groups of crystallins found in vertebrates (9), including the  $\alpha$ -,  $\beta$ -, and  $\gamma$ -crystallin families (11). Although  $\alpha$ -crystallin exhibits chaperone activity,  $\beta$ - and  $\gamma$ -crystallins have a largely structural function (7), providing the lens with the high refractive index required for clear vision (6, 12). Human  $\gamma$ D-crystallin (H $\gamma$ D-crys)<sup>2</sup> is the third most abundantly expressed  $\gamma$ -crystallin in the nucleus of the adult lens and accumulates in mature-onset cataracts. The x-ray crystal structure (Fig. 1A, PDB code 1HK0) (13) reveals that this 173-residue protein consists of a C-terminal domain (Ctd, blue) and N-terminal domain (Ntd, purple) joined by a seven-amino acid linker hinge. Both are composed of two  $\beta$ -sheet Greek key motifs, and they share a highly conserved hydrophobic interface (14). Biochemical studies have shown that the two domains exhibit different thermodynamic stability, with the Ctd being more stable than the Ntd. Parallel unfolding/refolding experiments of WT H $\gamma$ D-crys identified a partially folded intermediate in which the Ctd is native-like, but the Ntd is not fully folded (15, 16). Such a partially folded conformation initiated an irreversible aggregation pathway that competed with productive refolding under physiological conditions. The H $\gamma$ D-crys aggregates exhibited an ordered nature with a filamentous appearance (15). By contrast, when exposed to low pH, the resulting aggregates showed amyloid characteristics (17). In this vein, amyloid fibrils were also observed in recombinant mutant  $\gamma$ B-crystallin under physiological buffer conditions (18).

Although these biochemical assays have provided interesting morphological insights into the high molecular weight insoluble species (15, 17), the molecular basis governing the *in vitro* onset of H $\gamma$ D-crys polymerization (19) remains poorly understood (10). In this respect, recent molecular dynamics simulations have indeed postulated that H $\gamma$ D-crys may polymerize through successive domain swapping of the C-terminal  $\beta$  strands (20). However, direct experimental determination of such dimeric conformation remains elusive.

\* This work was supported by Marie Curie Intra-European Fellowships for Career Development Grant 329308 (to J. P. C.); Marie Curie Carrier Integration Grants 293462, Biotechnology and Biological Sciences Research Council Grant BB/J00992X/1, and Engineering and Physical Sciences Research Council Grant K00641X/1 (to S. G. M.); Royal Society Grant RG120038 (to S. G. M.); and National Institutes of Health Grants HL66030 and HL61228 (to J. M. F.). The authors declare that they have no conflicts of interest with the contents of this article. The content is solely the responsibility of the authors and does not necessarily represent the official views of the National Institutes of Health.

✂ Author's Choice—Final version free via Creative Commons CC-BY license.

<sup>1</sup> To whom correspondence should be addressed: Dept. of Physics and Randall Division of Cell and Molecular Biophysics, King's College London, London WC2R 2LS, UK. Tel.: 44-20-7848-7106; Fax: 44-20-7848-2430; E-mail: sergi.garcia-manyes@kcl.ac.uk.

<sup>2</sup> The abbreviations used are: H $\gamma$ D-crys, human  $\gamma$ D crystallin; Ctd, C-terminal domain; Ntd, N-terminal domain; AFM, atomic force microscopy.

Here we use a combination of molecular biology engineering techniques and single-molecule force spectroscopy AFM to characterize the unfolding mechanism of the multidomain H $\gamma$ D-crys protein. Single-molecule mechanical experiments have mapped the force-induced unfolding pathways of a wide variety of proteins along a well defined end-to-end reaction coordinate (21, 22). Crucially, these experiments have been able to identify misfolding events along the individual unfolding trajectories of topologically simple small proteins (23–27). By engineering H $\gamma$ D-crys polyprotein constructs in which the number of neighboring H $\gamma$ D-crys domains is changed rationally, we unambiguously identify a dimeric conformation in which two N termini  $\beta$  strands swapped. We hypothesize that such an elusive conformation might hold the key to explaining, from a single molecule perspective, the genesis of mature-onset cataracts, a widespread misfolding disease.

## Experimental Procedures

**Protein Engineering**—The polyproteins used in this work (H $\gamma$ D-crys-I27)<sub>4</sub>, (I27-Ntd)<sub>4</sub>, (I27-Ctd)<sub>4</sub>, [I27-(H $\gamma$ D-crys)<sub>2</sub>-I27], (HD-crys<sub>R14C</sub>-I27)<sub>4</sub>, [I27-(H $\gamma$ D-crys<sub>R14C</sub>)<sub>2</sub>-I27], and (H $\gamma$ D-crys-I27)<sub>2</sub> were subcloned using the BamHI, BglII, and KpnI restriction sites (28). The multidomain proteins were cloned into the pQE80L (Qiagen) expression vector and transformed into the BLRDE3 *Escherichia coli* expression strain. Cells were grown in Luria broth supplemented with 100  $\mu$ g/ml ampicillin at 37 °C. After reaching an A<sub>600</sub> of  $\sim$ 0.6, cultures were induced with 1 mM isopropyl 1-thio- $\beta$ -D-galactopyranoside and incubated overnight at 25 °C. Cells were disrupted with a French press, and the polyproteins from the lysate were purified by metal affinity chromatography on Talon resin (Takara, Clontech), followed by gel filtration using a Superdex 200 10/300 GL column (GE Biosciences). Proteins were stored in PBS buffer at 4 °C. The [I27-(H $\gamma$ D-crys)<sub>2</sub>-I27] polyprotein with a longer linker was constructed by adding the sequence GGC-TCTGGTTCAGGTTTCAGGAAGCGGCAGTGGTTCAGG-AAGC to the linker connecting both H $\gamma$ D-crys monomers.

**Force Spectroscopy**—Constant velocity atomic force microscopy experiments were conducted at room temperature using both a home-made setup described elsewhere (29) and a commercial Luigs and Neumann force spectrometer (30). In all cases, the sample was prepared by depositing 1–10  $\mu$ l of protein in PBS solution (at a concentration of 1–10 mg ml<sup>-1</sup>) onto a freshly evaporated gold coverslide. Each cantilever (Si<sub>3</sub>N<sub>4</sub> Bruker MLCT-AUHW) was calibrated individually using the equipartition theorem, giving rise to a typical spring constant of  $\sim$ 12 pN nm<sup>-1</sup>. Single proteins were picked up from the surface and pulled at a constant velocity of 400 nm s<sup>-1</sup>. Experiments were carried out in phosphate-buffered saline solution (pH 7.2).

**Data Analysis**—All data were recorded and analyzed using custom software written in Igor Pro 6.0 (Wavemetrics). For the experiments conducted with the [I27-(H $\gamma$ D-crys)<sub>2</sub>-I27], [I27-(H $\gamma$ D-crys<sub>R14C</sub>)<sub>2</sub>-I27], and [I27-(H $\gamma$ D-crys)]<sub>2</sub> proteins, only recordings showing the signature corresponding to the unfolding of both I27 modules were analyzed.

**Light Scattering**—Thermal unfolding of 0.6 mg/ml of the corresponding polyproteins was induced by incubation at 60 °C in

PBS buffer. Aggregation of each individual polyprotein was monitored by continuous measurement of light scattering at 350 nm in a Fluoromax 4 (Horiba) instrument.

## Results

**Nanomechanical Characterization of the Multidomain H $\gamma$ D-crys Protein**—A single polyprotein composed of four identical repeats of the H $\gamma$ D-crys monomer, each of them flanked by the well characterized I27th module of the titin protein (H $\gamma$ D-crys-I27)<sub>4</sub>, was tethered between the AFM cantilever tip and the gold substrate (Fig. 1B) and stretched at a constant velocity. The resulting unfolding trajectories (Fig. 1C) displayed a sawtooth pattern consisting of up to eight unfolding force peaks separated by an increment in contour length of  $\Delta L_c \sim$ 30 nm (Fig. 1D) corresponding to the unfolding of the H $\gamma$ D-crys that precedes the unfolding of the I27 molecular fingerprint (31). Crucially, the unfolding events clustered into two different levels of mechanical stability, of  $\sim$ 85 pN (*circles*) and  $\sim$ 125 pN (*stars*), as shown in Fig. 1E. The forces required to unfold the wild-type  $\gamma$ D-crystallin polyprotein are similar to the forces required to unfold the Ca<sup>2+</sup>-binding archaeal M-crystallin ( $\sim$ 90 pN) (31). Interestingly, the low-force unfolding domains often exhibit a weak ( $\sim$ 50 pN) mechanical intermediate with a related increment in contour length of  $\Delta L_c \sim$ 8 nm (Fig. 1C, *inset*). Because of the two-domain structure of the H $\gamma$ D-crys monomer (Fig. 1A), it is very likely that the two distinct levels of mechanical stability observed in Fig. 1 correspond to the independent, sequential unfolding of both domains (Ntd and Ctd). To unambiguously identify the origin of the low and high mechanical stability events, we individually tested the mechanical stability of the (I27-Ntd)<sub>4</sub> and (I27-Ctd)<sub>4</sub> polyproteins (Fig. 2, A and E, respectively). These experiments revealed that the low mechanical stability events (*blue circles*, Fig. 2B) correspond to the unfolding of the Ctd ( $\sim$ 96 pN, Fig. 2G), whereas the Ntd (*purple stars*) is more mechanically resilient (Fig. 2B), requiring  $\sim$ 136 pN (Fig. 2C) to unfold. Together, these experiments demonstrate that, at the pulling velocity of 400 nm s<sup>-1</sup>, the mechanical unfolding of the H $\gamma$ D-crys monomer occurs sequentially, where the Ctd unfolds first, followed by the unfolding of the more mechanically resilient Ntd. The close agreement between the measured unfolding forces for the complete H $\gamma$ D-crys monomer and for each of the truncated forms suggests that each domain remains stable on its own and unfolds independently after the disruption of the binding hydrophobic interface. This observation is surprising because it contrasts with chemical denaturation experiments demonstrating that the hydrophobic interface determines the relative stability of the C and N termini in  $\beta$ B2- and  $\gamma$ B-crystallin (32, 33). To further prove the putative mechanical role of the hydrophobic interface, we studied the mechanical stability of the polyprotein mutant containing the double mutation Gln-54/Gln-143, which has been described to chemically destabilize the hydrophobic interface (34). Our experiments demonstrate that the mechanical stability of the mutant protein does not differ from that of the wild-type protein (data not shown). The unfolding sequence observed in our nanomechanical experiments agrees with the predictions obtained by coarse grain simulations under force (35) and is in sharp contrast with the relative thermodynamic stability of

## A Domain-swapped Misfolded Conformation in H $\gamma$ D-crystallin

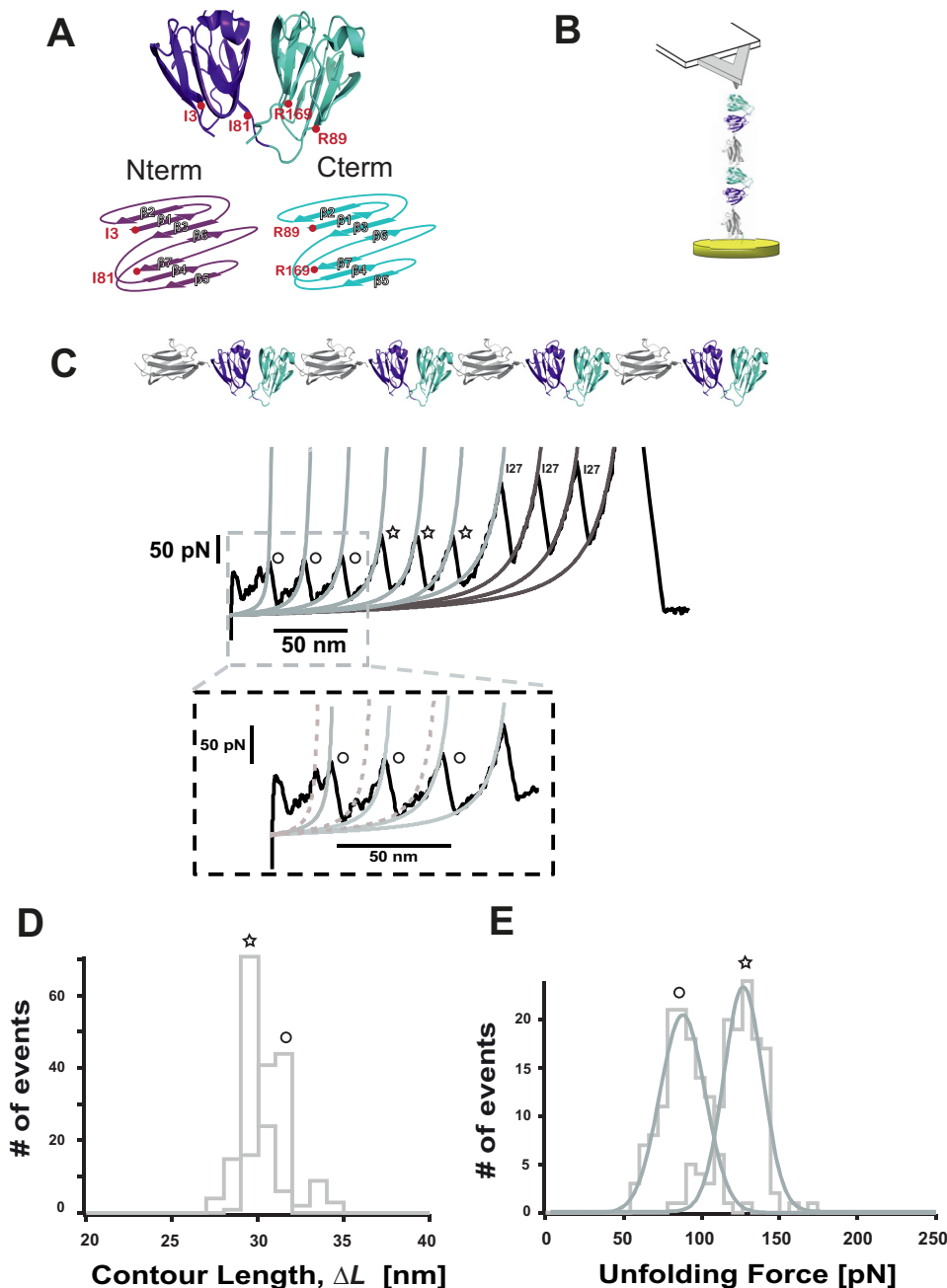


**FIGURE 1. The two domains of H $\gamma$ D-cryst unfold independently following a hierarchy in their mechanical stability.** *A*, structure of a H $\gamma$ D-cryst monomer. *Nterm*, N terminus; *Cterm*, C terminus. *B*, single-molecule AFM experiment layout. *C*, the unfolding trajectory of an individual (H $\gamma$ D-cryst-I27)<sub>4</sub> polyprotein follows a hierarchy in the mechanical stability whereby the low mechanical stability events (*circles*) unfold first (*D*) at  $84.7 \pm 14.50$  pN ( $n = 123$ ), followed by those exhibiting higher mechanical resistance (*stars*) at  $123.6 \pm 12.55$  pN ( $n = 127$ ). *E*, by contrast, both types of events cannot be singled out on the basis of their increment in contour length, which is in both cases  $\Delta L_c \sim 30$  nm ( $\Delta L_c = 29.1 \pm 0.62$  nm,  $n = 120$  (*stars*), and  $\Delta L_c = 30.4 \pm 0.8$  nm,  $n = 116$  (*circles*)).

both domains, showing that the Ctd is more stable than the Ntd (15).

*H $\gamma$ D-cryst* Forms a Misfolded, Domain-swapped Conformation—Protein aggregation requires, by definition, the physical interaction of individual monomers present in solution. To increase the effective monomer concentration in the context of a single polyprotein chain, we engineered a construct consisting of two neighboring (H $\gamma$ D-cryst) domains flanked by one I27 monomer at each side (Fig. 3*A*). Pulling on the resulting [I27-(H $\gamma$ D-cryst)<sub>2</sub>-I27] polyprotein results in two types of unfolding trajectory-

ries. In the majority of cases ( $\sim 85\%$ ), a “regular” unfolding is observed (Fig. 3*B*), following the same pattern as the (H $\gamma$ D-cryst-I27)<sub>4</sub> polyprotein, where the forces to unfold both the Ctd ( $\sim 97$  pN, Fig. 3*B*, *blue fits, circles*) and Ntd ( $\sim 137$  pN, Fig. 3*B*, *purple fits, stars*, and Fig. 3*C*) closely match the forces measured for each domain independently (Fig. 2, *C* and *G*). In addition to the expected 30-nm increment in contour length typically observed for both domains unfolding, in some instances, H $\gamma$ D-cryst unfolds eliciting shorter lengths, revealing the presence of low-probability alternative unfolding pathways (data not shown).

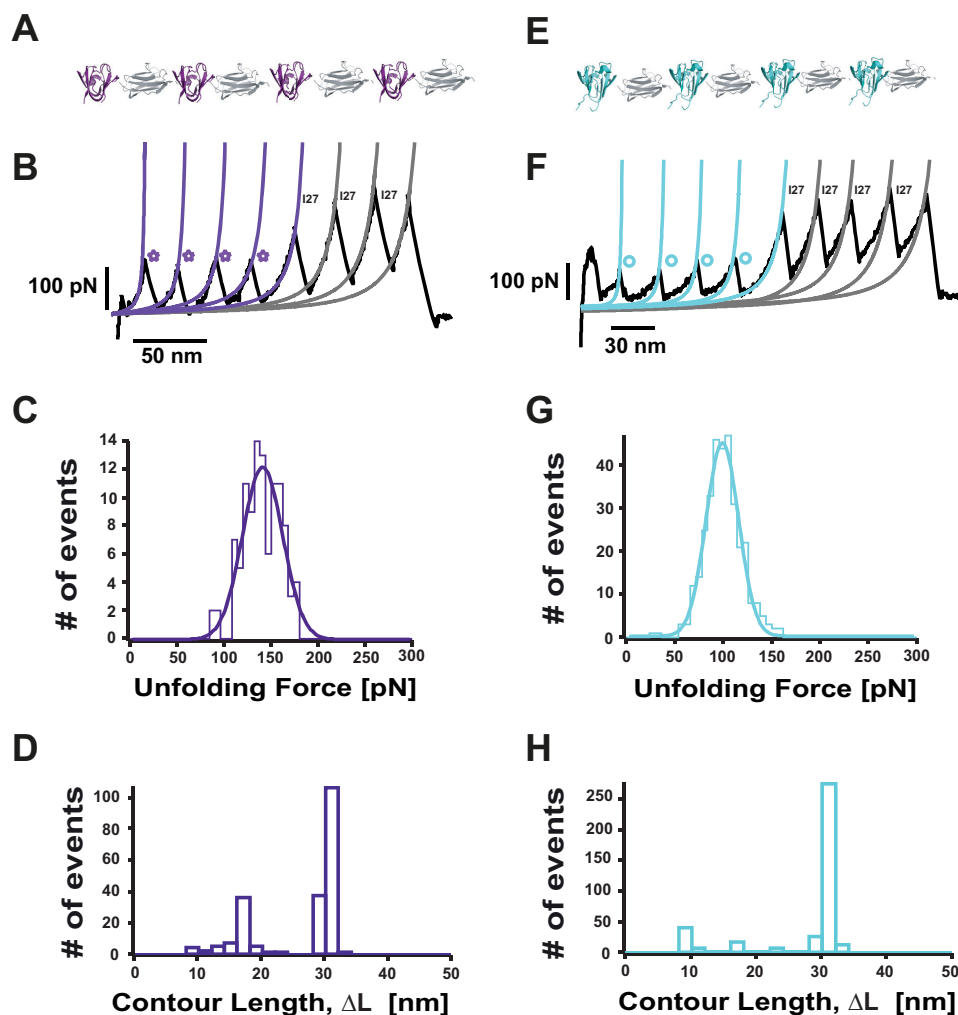


**FIGURE 2. The N terminus domain of H $\gamma$ D-crys exhibits a higher mechanical stability than the C terminus domain.** *A*, schematic of the (I27-Ntd)<sub>4</sub> polyprotein. *B*, typical force extension unfolding trajectory of a (I27-Ntd)<sub>4</sub> polyprotein, showing four unfolding peaks (purple stars) followed by the unfolding of the well characterized I27 protein (gray fits). *C*, distribution of unfolding forces for the Ntd, yielding an average unfolding force of  $136.2 \pm 18.0$  pN ( $n = 106$ ). *D*, distribution of the measured increment in contour length,  $\Delta L_c$ , upon unfolding ( $n = 217$ ). Although a main unfolding  $\Delta L_c$  of  $29.3 \pm 0.7$  nm is measured, other shorter  $\Delta L$  values are also evident, probably because of unfolding events of partially unfolded domains. *E*, schematic of the (I27-Ctd)<sub>4</sub> polyprotein. *F*, individual unfolding trajectory of an individual (I27-Ctd)<sub>4</sub> polyprotein, showing the unfolding of the Ctd first (blue circles and blue Worm-like chain fits), followed by the unfolding of the I27 protein (gray Worm-like chain fits). *G*, mechanical unfolding of an individual Ctd requires a force of  $96.1 \pm 16.8$  pN ( $n = 331$ ). *H*, the distribution of associated increment in contour length  $\Delta L_c$  values ( $n = 430$ ) shows a main unfolding  $\Delta L_c = 29.9 \pm 0.8$  nm together with and a much smaller population of events with associated shorter  $\Delta L_c$  values.

Surprisingly, in the remaining  $\sim 15\%$  of cases, the [I27-(H $\gamma$ D-crys)<sub>2</sub>-I27] polyprotein unfolds following an “anomalous” pattern (Fig. 3D). The first H $\gamma$ D-crys unfolding event is characterized by an unfolding force of 82 pN and an associated increment in contour length of  $\Delta L_1 \sim 30$  nm (Fig. 3, *E.1*), reminiscent of the unfolding of a Ctd (Fig. 3D, blue circle). This is followed by an unfolding event occurring at higher forces ( $\sim 120$  pN) (Fig. 3, *E.2*), close to the force value that is required to unfold an Ntd (Fig. 3D, purple star) and associated with an increment in contour length  $\Delta L_2$ . Notably, a clear unfolding peak of low mechanical stability ( $\sim 35$  pN) occurs next, releasing a protein length  $\Delta L_3 \sim 31$  nm (Fig. 3, *E.3*). The last H $\gamma$ D-crys unfolding event occurs at a force of  $\sim 95$  pN, again compatible with the unfolding of the second Ctd (Fig. 3D, blue circle,  $\Delta L_4 \sim 30$  nm) (Fig. 3, *E.4*). This unfolding pattern is evocative of a mechanism whereby at least one mechanically labile domain remains protected from the effect of force until a more resilient domain

unfolds first (36). In 12 of the 57 anomalous trajectories, the force corresponding to the unexpectedly low-stability peak is too low to be measured, in which case a large associated increment in contour length of  $(\Delta L_2 + \Delta L_3) \sim 67$  nm is measured after the unfolding of the Ntd. For the rest of the trajectories, application of the extended Kalman filter algorithm (37) provided rigorous, real-time estimates of  $\Delta L_3$ .

To explain the origin of the observed unfolding trajectories, we constructed a plausible schematic (Fig. 4). In the regular pattern (Fig. 4A), upon stretching the [I27-(H $\gamma$ D-crys)<sub>2</sub>-I27] polyprotein, all domains are immediately exposed to the pulling force. The unfolding sequence involves a first fast extension of both hinges connecting the Ntd and Ctd in each H $\gamma$ D-crys monomer together with the linker connecting both neighboring H $\gamma$ D-crys monomers. This is followed by the unfolding of both the Ctd and Ntd according to their relative mechanical stabilities.

## A Domain-swapped Misfolded Conformation in H $\gamma$ D-crystallin

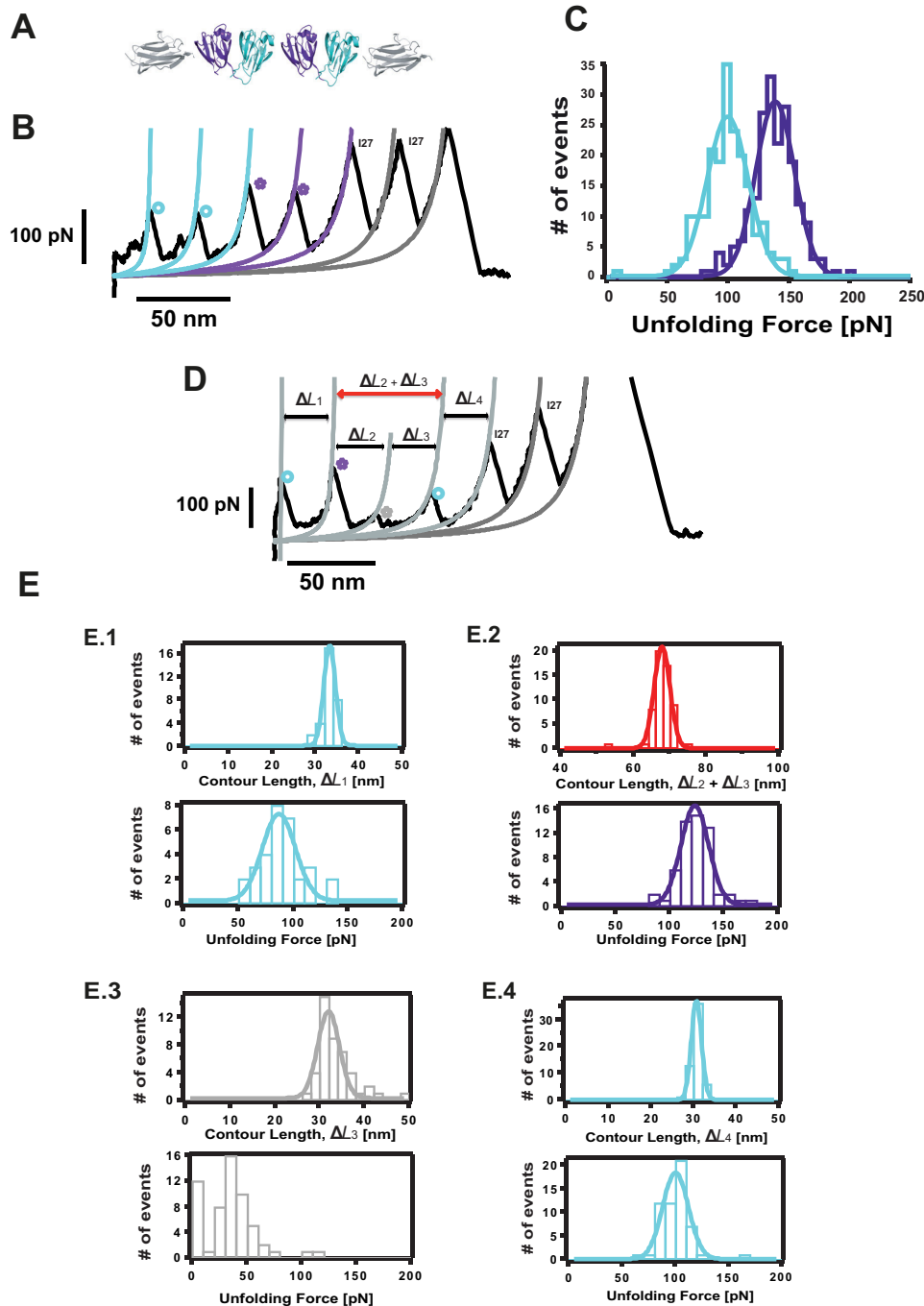


**FIGURE 3. Identification of a misfolded dimeric conformation in H $\gamma$ D-crys.** *A*, schematic of the constructed [I27-(H $\gamma$ D-crys)<sub>2</sub>-I27] polyprotein. Mechanical unfolding of this construct results in two main types of trajectories. *B*, in ~85% of instances, the Ctd (blue fit) unfolds first at  $96.7 \pm 17.0$  pN ( $n = 198$ ), followed by the unfolding of the Ntd (purple fit), at  $135.8 \pm 16.0$  pN ( $n = 201$ ) before the unfolding of the I27 marker occurring at  $251.9 \pm 34.0$  pN ( $n = 158$ ). *D*, in the remaining ~15% of trajectories ( $n = 57$ ), the [I27-(H $\gamma$ D-crys)<sub>2</sub>-I27] polyprotein unfolds in an anomalous fashion that is not consistent with a mechanical hierarchy scenario. *E*, a first unfolding peak (*E.1*) occurs at  $82.2 \pm 15.0$  pN ( $n = 31$ ) and  $\Delta L_1 = 32.3 \pm 1.3$  nm ( $n = 31$ ). The second unfolding peak (purple star) occurs at  $118.4 \pm 12.8$  pN and  $(\Delta L_2 + \Delta L_3) = 66.9 \pm 2.1$  nm; ( $n = 57$ , *E.2*). Next, a low mechanical stability peak of ~35 pN and  $\Delta L_3 = 31.0 \pm 2.4$  nm ( $n = 45$ ) is observed. Prior to the unfolding of the I27 internal controls, a last unfolding event, characterized by an unfolding force of  $95.3 \pm 12.1$  pN and a  $\Delta L_4 = 29.7 \pm 1.2$  nm ( $n = 56$ ), is observed (*E.4*).

Inspired by recent molecular dynamics simulations (20) and on the basis of the domain-swapped crystal structure of  $\beta$ B2-crystallin (38, 39), we first considered domain swapping as a putative structural motif that enables us to rationalize the origin of these anomalous unfolding trajectories that do not follow the classical sequential mechanical hierarchy scenario (36, 40). The observed trajectories are fully compatible with a simple

structural model where the swap occurs between the Ntds (Fig. 4*B*) and could not be explained when the swap occurred in the Ctd instead. According to this model, when stretching the swapped dimer, the mechanical force is first applied to Ntd1 and Ctd2 (Fig. 4*C*). Because of their different mechanical stabilities, Ctd2 has the highest probability to unfold first (Fig. 4*C*,  $\Delta L_1$ ). The force is then applied between the N and C termini of

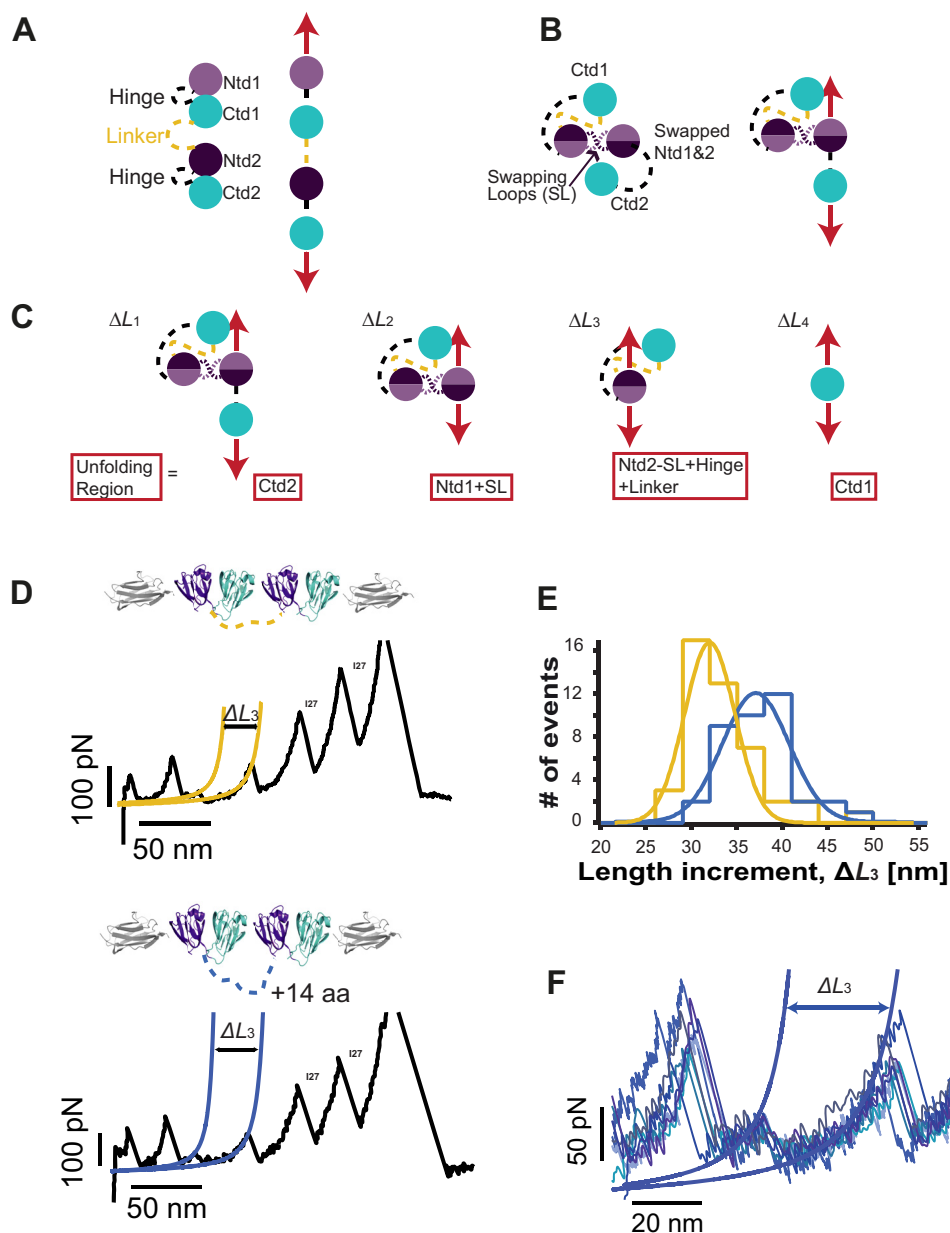


FIGURE 4. **A simple structural model compatible with stretching a domain-swapped conformation.** *A*, schematic explaining the regular unfolding trajectories. *B*, schematic of the polyprotein conformation compatible with the anomalous trajectories on the basis of Ntd domain swapping. When exposed to mechanical force (*red arrows*), this “swapped” conformation acts as a force-shielding element that prevents Ctd1 from being exposed to the mechanical force. *SL*, swapping loop. *C*, the force is first applied to the termini of Ctd2 and Ntd1. The unfolded and extended region is described in the *red frame* in each step along the sequence. *D*, pulling on the [I27-(H $\gamma$ D-crys)<sub>2</sub>-I27] polyprotein in which 14 extra residues, (GS)<sub>7</sub>, were added to the linker region (*dashed yellow lines*) displays swapped unfolding trajectories akin to those observed for the regular construct. *E*, comparing the increment in the protein contour length measured concomitant to the unfolding of the Ntd2 domain ( $\Delta L_3$ ) for the regular polyprotein construct (*yellow fit*,  $\Delta L_3 = 30.5 \pm 2.8$  nm,  $n = 45$ ) and for the longer linker polyprotein (*blue fit*,  $\Delta L_3 = 35.6 \pm 3.7$  nm,  $n = 38$ ) reveals a measured  $\sim 5.1$ -nm difference in length. *F*, pulling the longer linker polyprotein at a higher speed ( $1200$  nm s<sup>-1</sup>) provides a clearer and more accurate measurement of  $\Delta L_3$ .

the Ntd1 swapped structure (Fig. 4C,  $\Delta L_2$ ), which will trigger the whole Ntd1 to unfold and extend, together with an extra swapped linker (Fig. 4C, *dashed purple lines*). When unfolded, the force is applied directly to the remaining Ntd2 part of the swapped conformation. Unfolding and extending such an Ntd2 part of the swapped structure (Fig. 4C,  $\Delta L_3$ ) occurs concomitant to the extension of the hinge linker that connects the Ctd and Ntd in the structure (Fig. 4C, *black dashed lines*), and also the linker (Fig. 4C, *yellow dashed lines*) connecting both H $\gamma$ D-crys monomers within the polyprotein chain. Finally, the

remaining Ctd1 can unfold easily (Fig. 4C,  $\Delta L_4$ ). Notably, in this polyprotein chimera, the interdomain linker is the only engineered (and, therefore, non-native) part of the construct. Investigating the effects of changing the linker length on these misfolding trajectories would enable us to unambiguously pinpoint the exact position in the unfolding sequence where the linker extension takes place (Fig. 4B, *yellow dashed lines*), further testing our domain swap hypothesis.

To this end, we constructed an analogous polyprotein, [I27-(H $\gamma$ D-crys)<sub>2</sub>-I27], where 14 extra amino acids were added to

## A Domain-swapped Misfolded Conformation in H $\gamma$ D-crystallin

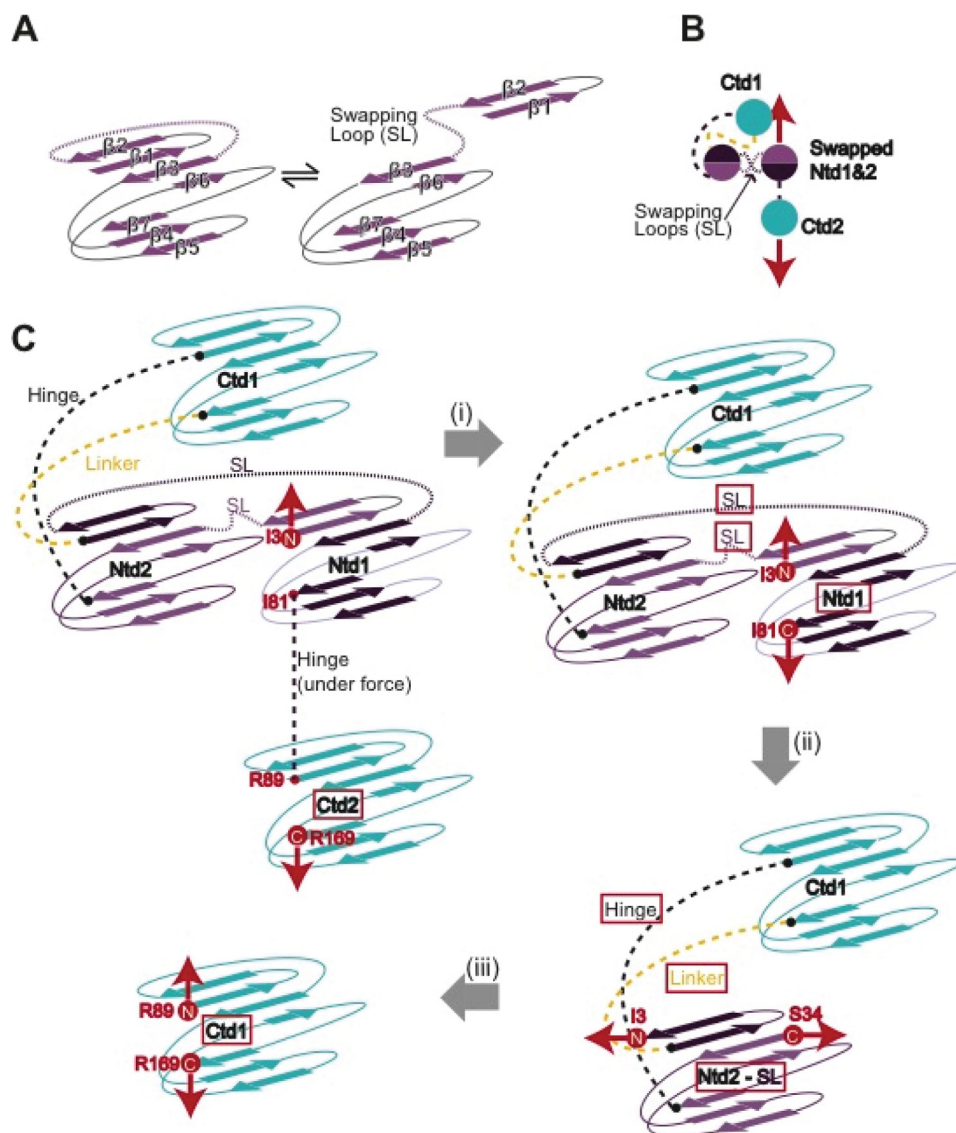


**FIGURE 5. The most probable swapping motif involves the  $\beta 1$  and  $\beta 2$  strands of the Ntd of H $\gamma$ D-crys.** *A*, topological model of the domain-swapped protein construct that identifies the swapping motifs between two Ntds (*B*) and highlights the sequence of structural rearrangements the polyprotein construct undergoes when exposed to mechanical force (*C*). After Ctd2 unfolding (*i*), the force is applied from the C-terminal of Ntd1 (I81) and the N terminus of the swapped conformation (I3). It is very possible that the swapping rearrangement accounts for the lower mechanostability ( $\sim 20$  pN) of this swapped Ntd1 domain with respect to a WT Ntd (Fig. 2). When the Ntd1-swapped motif unfolds and extends concomitant to the swapping loop, the force is directly applied to the new N(I3) and C(S34) termini of the Ntd2 swapped conformation (*ii*). Remarkably, the pulling direction has now changed, which readily explains the lower mechanical stability of Ntd2 of the swapped structure. This plausible structural model is consistent with the experimental traces we observed (Fig. 3D) in terms of the unfolding sequence, increment in contour length, and measured unfolding force.

the linker between both individual H $\gamma$ D-crys domains. Pulling on such a construct also showed domain-swapped trajectories (Fig. 4D) exhibiting an unfolding pattern akin to that observed for the [I27-(H $\gamma$ D-crys) $_2$ -I27] polyprotein with the regular (shorter) linker. Indeed, comparing  $\Delta L_3$  for both polyprotein constructs revealed that the unraveling of the Ntd2 swapped domain was  $\sim 5.1$  nm longer in the modified construct (Fig. 4E,  $\Delta L_3 \sim 35.6$  nm, *blue fit*), closely matching the expected length (14 amino acids  $\times 0.4$  nm/amino acid = 5.6 nm).

To precisely locate the position of the domain swap, we first took into account the following two structural considerations: in general, swapping motifs occur close to domain termini (41), and unstructured flexible regions lacking secondary structure enhance the swapping probability (4). We combined them with

our experimental observations. As shown in Fig. 4C, the measured length  $\Delta L_2$  corresponds to the unfolding and extension of Ntd1 together with the swapping loop (SL). According to our measurements,  $\Delta L_2 = (66.9 - 31.0) = 35.9$  nm. Because the increment in contour length associated with the unfolding of Ntd is  $\Delta L = 29.3$  nm (Fig. 2D), it follows that the swapping loop extension is 6.6 nm ( $35.9 - 29.3$  nm), involving 16 amino acids. Bearing all this in mind, a close inspection of the Ntd structure reveals that only the loop connecting the  $\beta 2$ - $\beta 3$  strands is composed of 15 amino acids (all other loops are significantly shorter), and is placed right at the N terminus of the crystallin Ntd. This suggests that  $\beta 1$ - $\beta 2$  strands, encompassing amino acids Ile-3 to Cys-18, form a structural motif that is a very likely candidate to swap (Fig. 5, *A* and *B*).

According to this hypothesis, we constructed a topological model for the domain-swapped protein construct that is consistent with our findings (Fig. 5C). This model clearly identifies the swapping motifs between two Ntds and highlights the sequence of structural rearrangements the polyprotein construct undergoes when exposed to mechanical force. Crucially, the model provides a visual representation of the points of application of force during each unfolding step. Remarkably, the mechanical stability of Ntd2 of the swapped structure ( $\sim 35$  pN) is significantly lower than that corresponding to the unfolding of the Ntd in the regular trajectories. According to our topological model (Fig. 5C), such a drastic change in mechanical resistance can be explained by a change in pulling direction. It is indeed well reported that the direction of force propagation has a strong effect on the mechanical stability of proteins (42–44). To prove the hypothesis, we constructed a circular permutant that mimics the pulling direction of Ntd2 in the context of the swapped trajectories. Mechanical unfolding of this circular permutant of Ntd2 (data not shown) confirmed the low mechanical stability of Ntd2 when the pulling direction was changed.

## Discussion

Using our polyprotein approach, we covalently linked two H $\gamma$ D-crys monomers, each of which was a multidomain protein with high sequence identity. Such strategy results in a high effective local protein concentration, *a priori* making it much more vulnerable to unfolding and aggregation (27, 45). Domain swapping has been identified as a general possible initial mechanism for protein misfolding (41, 46). Lacking the crystal structure, direct identification of these low-probability conformations remains challenging using traditional biophysical techniques. By contrast, single-molecule techniques are ideally suited to detect rare events (22, 26). In this vein, pioneering experiments using AFM revealed domain swapping-based misfolding events within individual polyproteins made out of eight identical repeating domains of the well characterized I27th module of the giant protein titin, (I27) $_8$  (23). These results were further supported by single molecule FRET experiments, suggesting that sequence diversity might be an evolutionary strategy to avoid misfolding in multidomain proteins (27, 47).

Our single-molecule experiments readily identified a previously elusive domain-swapped H $\gamma$ D-crys dimer conformation. On the basis of the independent unfolding of both domains in the multidomain protein, both exhibiting distinct mechanical stabilities, and according to their unfolding sequence within the swapped form, we suggest that the swapped element most likely corresponds to the  $\beta 1$  and  $\beta 2$  strands of the N terminus domain. At this point, we cannot rule out the possibility that the swapping motif encompasses the terminal  $\beta 7$  strand instead. In this case, the swapping loop linking the  $\beta 7$  strand with  $\beta 6$  would also be composed of 15 amino acids. However, the fact that the loop has secondary structure ( $\alpha$  helix), together with the observation that the  $\beta 1$  and  $\beta 2$  strands exhibit the higher B-factor (suggesting the lowest stability, PDB code 1HK0) within the Ntd, strongly favors the hypothesis of  $\beta 1$  and  $\beta 2$  strands, encompassing amino acids Ile-3 to Cys-18, being, in fact, the swapping motif.

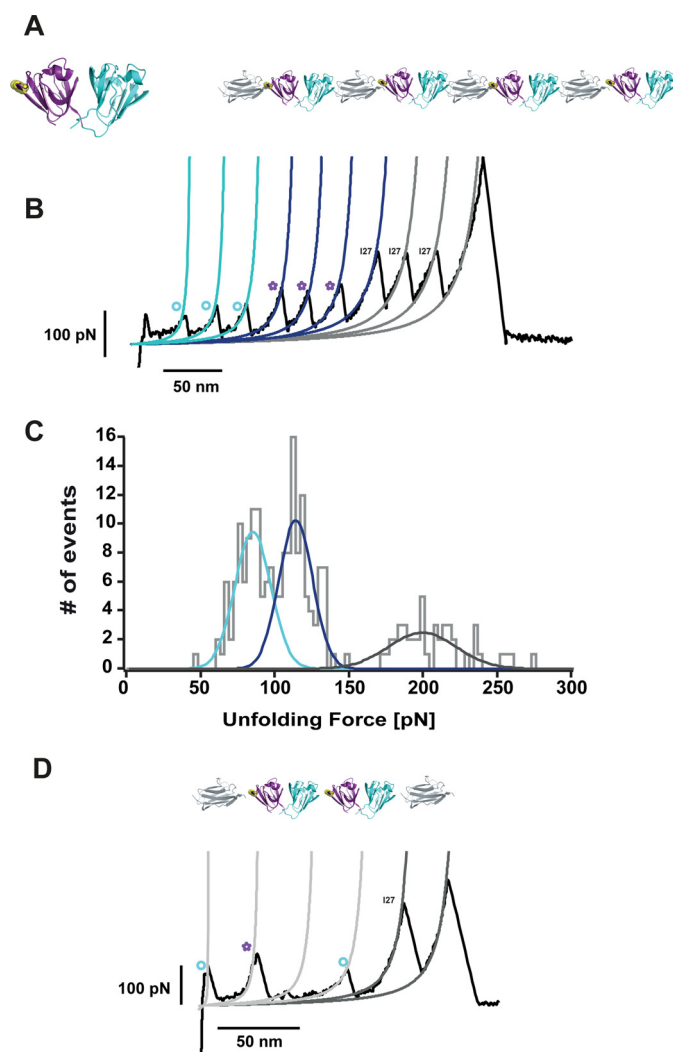


**FIGURE 6. The R14C mutation exhibits misfolding trajectories akin to those corresponding to the wild-type H $\gamma$ D-crys.** A, the mechanical stability of the (I27-H $\gamma$ D-crys<sub>R14C</sub>) $_4$  polyprotein exhibits the same unfolding pattern (B) as the wild-type (I27-H $\gamma$ D-crys) $_4$  polyprotein. C, the Ctd unfolds first at  $83.7 \pm 12.2$  pN (blue fits, circles), followed by the unfolding of the Ntd at  $112.6 \pm 7.28$  pN (purple fits, stars). Finally, the I27 modules unfold at higher forces,  $197.9 \pm 22.9$  pN (gray fits). D, to investigate whether the R14C mutation triggered misfolding mechanisms that differ from that observed for the wild-type protein, we engineered the [I27-(H $\gamma$ D-crys<sub>R14C</sub>) $_2$ -I27] polyprotein. Akin to the wild-type case, the misfolding trajectories were reminiscent of a domain swap scenario. In these single-molecule experiments, we did not identify any other alternative misfolding mechanism, probably induced by the putative presence of a disulfide bond.

These results are in contrast with molecular dynamics simulations that identify a domain-swapped structure that occurs within the Ctd instead (20). For the swap to occur, the Ntd of the protein has first to unfold, at least partially (Fig. 5A). In this vein, it is intriguing that most of the congenital cataractogenic mutations in the  $\gamma$ -crystallins (T4P, L5S/F9S, R14C, P23S/P23T, W42R, V75D, and R76R), which readily trigger the protein to unfold, occur in the N terminus (10, 48–51); incidentally, a great number of these occur within the  $\beta 1$  and  $\beta 2$  strands. In particular, the R14C mutation has been described to trigger juvenile-onset cataract, in which aggregation is thought to occur through disulfide bonds between adjacent domains (50). To investigate whether such a distinct aggregation mechanism could be identified at the single-molecule level, we con-

## A Domain-swapped Misfolded Conformation in H $\gamma$ D-crystallin

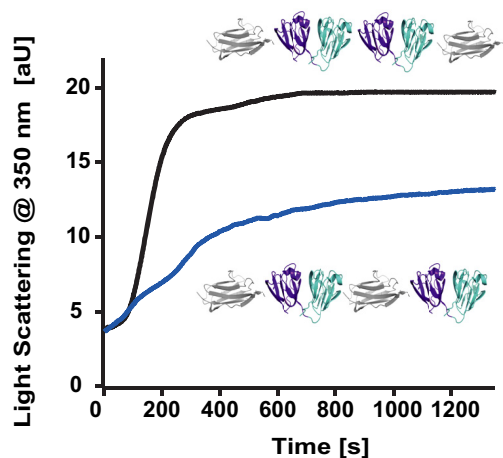


FIGURE 7. **Kinetics of light scattering at 350 nm.** The [I27-(H $\gamma$ D-crys)<sub>2</sub>-I27] polyprotein (black) aggregates more (and faster) than the related (H $\gamma$ D-crys-I27)<sub>2</sub> polyprotein.

structured the (I27-H $\gamma$ D-crys<sub>R14C</sub>)<sub>4</sub> and [I27-(H $\gamma$ D-crys<sub>R14C</sub>)<sub>2</sub>-I27] polyproteins, the latter with two H $\gamma$ D-crys<sub>R14C</sub> flanking monomers. Pulling on these proteins (Fig. 6) provided similar results as the wild-type protein. Crucially, although anomalous trajectories consistent with a domain-swapped conformation were also captured with similar probability, no further misfolding mechanisms compatible with a putative disulfide bond, which would significantly shorten the protein extensibility, were observed. Qualitatively, our results point toward the same direction as the biochemical experiments conducted in the bulk that postulate the presence of a swapped conformation with a folded Ctd and a partially (un)folded Ntd. It is interesting to point out that, for the swap to occur, the mechanically resistant Ntd needs to partially unfold. Bulk experiments have indeed demonstrated that the Ntd has a lower thermodynamic stability than the Ctd counterpart. However, the stability of these domains is context-specific (33), and slight variations in the relative stability of both domains, often through particular mutations, might ultimately determine the probability for the domain swap to occur.

More generically, domain swapping has been identified as a general possible initial mechanism for protein misfolding (41, 46), often being the conformational seed for the aggregation of a variety of proteins, including the human prion protein (52),  $\beta$ 2-microglobulin (53, 54), cystatin C (55), amyotrophic lateral sclerosis (1), and antitrypsin deficiency (2). Therefore, it is tempting to speculate that the domain-swapped conformations we identified at the single-molecule level could exhibit a higher propensity to aggregate. To test this hypothesis, we conducted aggregation bulk assays in which we measured the light scattering of the [I27-(H $\gamma$ D-crys)<sub>2</sub>-I27] polyprotein as a function of time and compared it with the value corresponding to the homologous [I27-(H $\gamma$ D-crys)]<sub>2</sub> polyprotein, where each H $\gamma$ D-crys is separated by an I27 module (Fig. 7). These results show a higher tendency to aggregate than the constructs composed of two H $\gamma$ D-crys neighboring domains.

It is premature to conclude that the previously elusive domain-swapped conformation we identify is the unique cause for the aggregation. However, the analysis of human cataracts

reveals the presence of insoluble species that are not structured precipitates but, rather, resemble the aggregates and polymers of partially folded intermediates associated with inclusion bodies or other forms of protein misfolding (5, 56). Therefore, it is at least enticing to hypothesize that the swapped dimer we captured at the single-molecule level might represent the onset seed of a particular (perhaps one of many) polymerization pathway leading to high molecular weight species associated with cataracts. Lacking structural characterization, probably because of the fast aggregation kinetics and the dynamic nature of the system, our experiments provide a structural insight into the first stages of misfolding that evaded capture using ensemble techniques. Together, our results provide a new piece in the puzzle of understanding the early mechanisms underlying protein misfolding occurring at the single-molecule level.

**Author Contributions**—S. G. M. and J. M. F. designed the research. S. G. M. and A. E. M. B. performed the AFM experiments. C. B. and A. L. conducted molecular biology. D. G. contributed to the structural model. J. P. C. conducted the aggregation experiments. S. G. M. analyzed the data and wrote the paper. All authors contributed to revising and editing the manuscript.

**Acknowledgments**—We thank Jonathan King (Massachusetts Institute of Technology) and Jorge Alegre-Cebollada (Centro Nacional de Investigaciones Cardiovasculares, Spain) for helpful discussions and Daniel Echelman (Columbia University) for critical reading of the manuscript.

### References

1. Mulligan, V. K., and Chakrabarty, A. (2013) Protein misfolding in the late-onset neurodegenerative diseases: common themes and the unique case of amyotrophic lateral sclerosis. *Proteins* **81**, 1285–1303
2. Carrell, R. W., and Lomas, D. A. (2002)  $\alpha$ 1-antitrypsin deficiency: a model for conformational diseases. *N. Engl. J. Med.* **346**, 45–53
3. Yamasaki, M., Sendall, T. J., Pearce, M. C., Whisstock, J. C., and Huntington, J. A. (2011) Molecular basis of  $\alpha$ 1-antitrypsin deficiency revealed by the structure of a domain-swapped trimer. *EMBO Rep.* **12**, 1011–1017
4. Liu, Y., and Eisenberg, D. (2002) 3D domain swapping: as domains continue to swap. *Protein Sci.* **11**, 1285–1299
5. Wang, Y., and King, J. (2010) in *Protein Misfolding Diseases: Current and Emerging Principles and Therapies* (Ramirez-Alvarado, M., Kelly, J. W., and Dobson, C. M., eds.), pp. 487–515, Wiley, Hoboken, New Jersey
6. Slingsby, C., Wistow, G. J., and Clark, A. R. (2013) Evolution of crystallins for a role in the vertebrate eye lens. *Protein Sci.* **22**, 367–380
7. Slingsby, C., and Wistow, G. J. (2014) Functions of crystallins in and out of lens: roles in elongated and post-mitotic cells. *Prog. Biophys. Mol. Biol.* **115**, 52–67
8. Moreau, K. L., and King, J. A. (2012) Protein misfolding and aggregation in cataract disease and prospects for prevention. *Trends Mol. Med.* **18**, 273–282
9. Slingsby, C., and Clout, N. J. (1999) Structure of the crystallins. *Eye* **13**, 395–402
10. Serebryany, E., and King, J. A. (2014) The  $\beta\gamma$ -crystallins: native state stability and pathways to aggregation. *Prog. Biophys. Mol. Biol.* **115**, 32–41
11. Hejtmanec, J. F. (2008) Congenital cataracts and their molecular genetics. *Semin. Cell Dev. Biol.* **19**, 134–149
12. Graw, J. (2009) Genetics of crystallins: cataract and beyond. *Exp. Eye Res.* **88**, 173–189
13. Basak, A., Bateman, O., Slingsby, C., Pande, A., Asherie, N., Ogun, O., Benedek, G. B., and Pande, J. (2003) High-resolution X-ray crystal structures of human  $\gamma$ D crystallin (1.25 Å) and the R58H mutant (1.15 Å) associated with aculeiform cataract. *J. Mol. Biol.* **328**, 1137–1147

14. Flaugh, S. L., Kosinski-Collins, M. S., and King, J. (2005) Contributions of hydrophobic domain interface interactions to the folding and stability of human  $\gamma$ D-crystallin. *Protein Sci.* **14**, 569–581
15. Kosinski-Collins, M. S., and King, J. (2003) *In vitro* unfolding, refolding, and polymerization of human  $\gamma$ D crystallin, a protein involved in cataract formation. *Protein Sci.* **12**, 480–490
16. Kosinski-Collins, M. S., Flaugh, S. L., and King, J. (2004) Probing folding and fluorescence quenching in human  $\gamma$  D crystallin Greek key domains using triple tryptophan mutant proteins. *Protein Sci.* **13**, 2223–2235
17. Papanikolopoulou, K., Mills-Henry, I., Thol, S. L., Wang, Y., Gross, A. A., Kirschner, D. A., Decatur, S. M., and King, J. (2008) Formation of amyloid fibrils *in vitro* by human  $\gamma$ D-crystallin and its isolated domains. *Mol. Vis.* **14**, 81–89
18. Sandilands, A., Hutcheson, A. M., Long, H. A., Prescott, A. R., Vrensen, G., Löster, J., Klopp, N., Lutz, R. B., Graw, J., Masaki, S., Dobson, C. M., MacPhee, C. E., and Quinlan, R. A. (2002) Altered aggregation properties of mutant  $\gamma$ -crystallins cause inherited cataract. *EMBO J.* **21**, 6005–6014
19. Mohr, B. G., Dobson, C. M., Garman, S. C., and Muthukumar, M. (2013) Electrostatic origin of *in vitro* aggregation of human  $\gamma$ -crystallin. *J. Chem. Phys.* **139**, 121914
20. Das, P., King, J. A., and Zhou, R. (2011) Aggregation of  $\gamma$ -crystallins associated with human cataracts via domain swapping at the C-terminal  $\beta$ -strands. *Proc. Natl. Acad. Sci. U.S.A.* **108**, 10514–10519
21. Fisher, T. E., Oberhauser, A. F., Carrion-Vazquez, M., Marszalek, P. E., and Fernandez, J. M. (1999) The study of protein mechanics with the atomic force microscope. *Trends Biochem. Sci.* **24**, 379–384
22. Fernandez, J. M., Garcia-Manyes, S., and Dougan, L. (2010) Force-clamp spectroscopy of single proteins. *Springer Ser. Chem. Ph.* **96**, 317–335
23. Oberhauser, A. F., Marszalek, P. E., Carrion-Vazquez, M., and Fernandez, J. M. (1999) Single protein misfolding events captured by atomic force microscopy. *Nat. Struct. Biol.* **6**, 1025–1028
24. Dougan, L., Li, J., Badilla, C. L., Berne, B. J., and Fernandez, J. M. (2009) Single homopolyptide chains collapse into mechanically rigid conformations. *Proc. Natl. Acad. Sci. U.S.A.* **106**, 12605–12610
25. Yu, H., Liu, X., Neupane, K., Gupta, A. N., Brigley, A. M., Solanki, A., Sosova, I., and Woodside, M. T. (2012) Direct observation of multiple misfolding pathways in a single prion protein molecule. *Proc. Natl. Acad. Sci. U.S.A.* **109**, 5283–5288
26. Borgia, A., Williams, P. M., and Clarke, J. (2008) Single-molecule studies of protein folding. *Annu. Rev. Biochem.* **77**, 101–125
27. Borgia, M. B., Borgia, A., Best, R. B., Steward, A., Nettels, D., Wunderlich, B., Schuler, B., and Clarke, J. (2011) Single-molecule fluorescence reveals sequence-specific misfolding in multidomain proteins. *Nature* **474**, 662–665
28. Carrion-Vazquez, M., Oberhauser, A. F., Fowler, S. B., Marszalek, P. E., Broedel, S. E., Clarke, J., and Fernandez, J. M. (1999) Mechanical and chemical unfolding of a single protein: a comparison. *Proc. Natl. Acad. Sci. U.S.A.* **96**, 3694–3699
29. Schlierf, M., Li, H., and Fernandez, J. M. (2004) The unfolding kinetics of ubiquitin captured with single-molecule force-clamp techniques. *Proc. Natl. Acad. Sci. U.S.A.* **101**, 7299–7304
30. Popa, I., Kosuri, P., Alegre-Cebollada, J., Garcia-Manyes, S., and Fernandez, J. M. (2013) Force dependency of biochemical reactions measured by single-molecule force-clamp spectroscopy. *Nat. Protoc.* **8**, 1261–1276
31. Ramanujam, V., Kotamarthi, H. C., and Ainavarapu, S. R. K. (2014)  $\text{Ca}^{2+}$  binding enhanced mechanical stability of an archaeal crystallin. *PLoS ONE* **9**, e94513
32. Mayr, E. M., Jaenicke, R., and Glockshuber, R. (1994) Domain interactions and connecting peptides in lens crystallins. *J. Mol. Biol.* **235**, 84–88
33. Mayr, E. M., Jaenicke, R., and Glockshuber, R. (1997) The domains in  $\gamma$ B-crystallin: identical fold-different stabilities. *J. Mol. Biol.* **269**, 260–269
34. Flaugh, S. L., Kosinski-Collins, M. S., and King, J. (2005) Interdomain side-chain interactions in human  $\gamma$ D crystallin influencing folding and stability. *Protein Sci.* **14**, 2030–2043
35. Sikora, M., and Cieplak, M. (2011) Mechanical stability of multidomain proteins and novel mechanical clamps. *Proteins* **79**, 1786–1799
36. Peng, Q., and Li, H. (2009) Domain insertion effectively regulates the mechanical unfolding hierarchy of elastomeric proteins: toward engineering multifunctional elastomeric proteins. *J. Am. Chem. Soc.* **131**, 14050–14056
37. Fernandez, V. I., Kosuri, P., Parot, V., and Fernandez, J. M. (2009) Extended Kalman filter estimates the contour length of a protein in single molecule atomic force microscopy experiments. *Rev. Sci. Instrum.* **80**, 113104
38. Bax, B., Lapatto, R., Nalini, V., Driessen, H., Lindley, P. F., Mahadevan, D., Blundell, T. L., and Slingsby, C. (1990) X-ray analysis of  $\beta$ B2-crystallin and evolution of oligomeric lens proteins. *Nature* **347**, 776–780
39. Itoh, K., and Sasai, M. (2008) Cooperativity, connectivity, and folding pathways of multidomain proteins. *Proc. Natl. Acad. Sci. U.S.A.* **105**, 13865–13870
40. Li, H., and Fernandez, J. M. (2003) Mechanical design of the first proximal Ig domain of human cardiac titin revealed by single molecule force spectroscopy. *J. Mol. Biol.* **334**, 75–86
41. Bennett, M. J., Schlunegger, M. P., and Eisenberg, D. (1995) 3D domain swapping: a mechanism for oligomer assembly. *Protein Sci.* **4**, 2455–2468
42. Carrion-Vazquez, M., Li, H., Lu, H., Marszalek, P. E., Oberhauser, A. F., and Fernandez, J. M. (2003) The mechanical stability of ubiquitin is linkage dependent. *Nat. Struct. Biol.* **10**, 738–743
43. Dietz, H., Berkemeier, F., Bertz, M., and Rief, M. (2006) Anisotropic deformation response of single protein molecules. *Proc. Natl. Acad. Sci. U.S.A.* **103**, 12724–12728
44. Brockwell, D. J., Paci, E., Zinober, R. C., Beddard, G. S., Olmsted, P. D., Smith, D. A., Perham, R. N., and Radford, S. E. (2003) Pulling geometry defines the mechanical resistance of a  $\beta$ -sheet protein. *Nat. Struct. Biol.* **10**, 731–737
45. Han, J. H., Batey, S., Nickson, A. A., Teichmann, S. A., and Clarke, J. (2007) The folding and evolution of multidomain proteins. *Nat. Rev. Mol. Cell Biol.* **8**, 319–330
46. Rousseau, F., Schymkowitz, J. W., and Itzhaki, L. S. (2003) The unfolding story of three-dimensional domain swapping. *Structure* **11**, 243–251
47. Wright, C. F., Teichmann, S. A., Clarke, J., and Dobson, C. M. (2005) The importance of sequence diversity in the aggregation and evolution of proteins. *Nature* **438**, 878–881
48. Jung, J., Byeon, I. J., Wang, Y., King, J., and Gronenborn, A. M. (2009) The Structure of the cataract-causing P23T mutant of human  $\gamma$  D-crystallin exhibits distinctive local conformational and dynamic changes. *Biochemistry* **48**, 2597–2609
49. Pande, A., Annunziata, O., Asherie, N., Ogun, O., Benedek, G. B., and Pande, J. (2005) Decrease in protein solubility and cataract formation caused by the Pro23 to Thr mutation in human  $\gamma$  D-crystallin. *Biochemistry* **44**, 2491–2500
50. Pande, A., Pande, J., Asherie, N., Lomakin, A., Ogun, O., King, J. A., Lubsen, N. H., Walton, D., and Benedek, G. B. (2000) Molecular basis of a progressive juvenile-onset hereditary cataract. *Proc. Natl. Acad. Sci. U.S.A.* **97**, 1993–1998
51. Santhiya, S. T., Shyam Manohar, M., Rawley, D., Vijayalakshmi, P., Namperumalsamy, P., Gopinath, P. M., Löster, J., and Graw, J. (2002) Novel mutations in the  $\gamma$ -crystallin genes cause autosomal dominant congenital cataracts. *J. Med. Genet.* **39**, 352–358
52. Knaus, K. J., Morillas, M., Swietnicki, W., Malone, M., Surewicz, W. K., and Yee, V. C. (2001) Crystal structure of the human prion protein reveals a mechanism for oligomerization. *Nat. Struct. Biol.* **8**, 770–774
53. Eakin, C. M., Attenello, F. J., Morgan, C. J., and Miranker, A. D. (2004) Oligomeric assembly of native-like precursors precedes amyloid formation by  $\beta$ -2 microglobulin. *Biochemistry* **43**, 7808–7815
54. Liu, C., Sawaya, M. R., and Eisenberg, D. (2011)  $\beta$ 2-Microglobulin forms three-dimensional domain-swapped amyloid fibrils with disulfide linkages. *Nat. Struct. Mol. Biol.* **18**, 49–55
55. Wahlbom, M., Wang, X., Lindström, V., Carlemalm, E., Jaskolski, M., and Grubb, A. (2007) Fibrillogenic oligomers of human cystatin C are formed by propagated domain swapping. *J. Biol. Chem.* **282**, 18318–18326
56. Wetzel, R. (1994) Mutations and off-pathway aggregation of proteins. *Trends Biotechnol.* **12**, 193–198

## Single-molecule Force Spectroscopy Predicts a Misfolded, Domain-swapped Conformation in human $\gamma$ D-Crystallin Protein

Sergi Garcia-Manyes, David Giganti, Carmen L. Badilla, Ainhoa Lezamiz, Judit Perales-Calvo, Amy E. M. Beedle and Julio M. Fernández

*J. Biol. Chem.* 2016, 291:4226-4235.

doi: 10.1074/jbc.M115.673871 originally published online December 24, 2015

---

Access the most updated version of this article at doi: [10.1074/jbc.M115.673871](https://doi.org/10.1074/jbc.M115.673871)

### Alerts:

- [When this article is cited](#)
- [When a correction for this article is posted](#)

[Click here](#) to choose from all of JBC's e-mail alerts

This article cites 55 references, 12 of which can be accessed free at <http://www.jbc.org/content/291/8/4226.full.html#ref-list-1>